Heliyon 10 (2024) e38818

Contents lists available at ScienceDirect

Heliyon

journal homepage: www.cell.com/heliyon

Research article

Chongrenside D from Smilax china L protects against inflammation-induced joint destruction via inhibiting osteoclastogenesis

Yanxiang Liang [a,b], Tian Qin [b], Caixia Pang [a], Xinru Yang [b], Zongbin Wu [a], Xiaolian Liao [b], Jie Zhang [c], Siyu Zeng [d,***], Chun Zhou [b,**], Cuiling Liu [a,*]

[a] Department of Pharmacy, Shenzhen Bao'an Traditional Chinese Medicine Hospital, Shenzhen, 518101, China
[b] School of Pharmaceutical Sciences, Guangdong Provincial Key Laboratory of Shock and Microcirculation, Southern Medical University, Guangzhou, 510515, China
[c] Department of Pharmacy, Guangdong Provincial Hospital of Chinese Medicine. the Second Affiliated Hospital of Guangzhou University of Chinese Medicine, 111 Dade Road, Guangzhou, 510120, China
[d] Department of Pharmacy, The Affiliated Guangdong Second Provincial General Hospital of Jinan University, Guangzhou, 510317, China

ARTICLE INFO

Keywords:
Chongrenside D
Osteoclast
LPS-Induced osteolysis
MAPK

ABSTRACT

Background: Bone-destructive diseases including rheumatoid arthritis (RA), osteoporosis, and bone metastases, are increasingly prevalent and worrisome due to the over-activated of osteoclasts. Chongrenside D (CGD) is a furostanol saponin extracted from Smilax china L, which has been demonstrated to have anti-inflammatory properties in our previous research. However, its effect on rheumatoid arthritis, especially on osteoclast differentiation and bone destruction has not yet been investigated.

Methods: We evaluated the toxicity of CGD on the cell we used, RANKL-induced osteoclast formation, bone resorption activity, and osteoclast-specific genes or protein expression using bone marrow-derived monocytes (BMMs) -derived osteoclasts. Furthermore, the protective function of CGD on the paws of osteolytic mice was carried out using micro-CT, H&E, TRAP staining, as well as real-time PCR, and western blotting. Inflammatory cytokine levels were conducted through ELISA assay. The relative signaling pathways were investigated using western blotting, immunofluorescence microscopy and real-time PCR.

Results: CGD notably inhibited RANKL-induced osteoclast formation, and suppressed the expression of osteoclast markers and actin ring formation, thus attenuating its bone resorption activity. For in vivo work, CGD protected against joint bone destruction induced by LPS, increased trabecular number and thickness, and reduced trabecular separation. CGD also inhibited the levels of inflammatory cytokines IL-6and TNF-α, improved the integrity of joint bones and decreased TRAP-positive staining area. The mechanistic study indicated that CGD down-regulated MMP9 and FAK-Src signaling, which were crucial for the resorption function of

* Corresponding author. Shenzhen Bao'an Traditional Chinese Medicine Hospital, Shenzhen, 518101, China.
** Corresponding author. SMU-KI United Medical Inflammatory Center, School of Pharmaceutical Sciences, Southern Medical University, No. 1023Shatai South Road, Baiyun District, Guangzhou, 510515, China.
*** Corresponding author. Deparment of Pharmacy, Guangdong Second Provincial General Hospital, No. 466 Xingang Middle Road, Haizhu District, Guangzhou, 510317, China.
E-mail addresses: cosmo81@qq.com (S. Zeng), zhouch@smu.edu.cn (C. Zhou), liucuiling0912@163.com (C. Liu).

https://doi.org/10.1016/j.heliyon.2024.e38818
Received 30 January 2024; Received in revised form 6 September 2024; Accepted 30 September 2024
Available online 1 October 2024

osteoclasts. CGD also inhibited MAPK pathway-mediated cell differentiation and survival, finally resulting in weak osteoclastogenesis.
Conclusion: CGD exerts a significant anti-osteolytic activity both in vitro and in vivo by inhibiting RANKL-induced osteoclastogenesis and function. Consequently, our study indicated that CGD may have a potential therapeutic role in the precaution of osteolytic bone disease.

1. Introduction

Bone homeostasis refers to the balance between osteoblasts, osteoclasts, and osteocytes, which is regulated by hormones. However, various osteolytic diseases disrupt this balance by increasing osteoclast numbers and enhancing bone resorption, such as osteoporosis, osteoarthritis-related bone destruction and solid tumors [1]. Langdahl BL summarized that these conditions present significant health challenges, and the currently available anti-osteoporosis drugs are often associated with serious side effects, including musculoskeletal pain, ocular inflammation, esophageal cancer, osteonecrosis of the jaw, and atypical fractures [2]. Thus, the development of safe alternative treatments for osteolytic diseases is an urgent issue.

Osteoclasts are derived from monocyte precursor cells and act as the only giant multinucleated cells in vivo that mediate bone resorption, leading to osteopenia. We previously reported that osteoclasts specifically express tartrate-resistant acid phosphatase (TRAP), which attaches to the bone surface by forming an actin-ring [3]. This enables the release of proteases, such as Cathepsin K and matrix metalloproteinase 9 (MMP-9), which facilitate the degradation of the mineralized bone matrix [4]. Boyle WJ, et al. acknowledged that the degradation products, like collagen fragments and solubilized calcium and phosphate, are processed within the osteoclast and released into circulation [5].

Macrophage colony-stimulating factor (M-CSF) and Receptor Activator of Nuclear Factor-κ B Ligand (RANKL) are crucial factors for osteoclastogenesis, and their roles during lineage allocation and maturation have been established. M-CSF promotes the differentiation and maturation of myeloid precursors and enhances the expression of RANKL in myeloid cells. While RANKL is an essential cytokine required for the fusion of monocytes, which can form multinucleated osteoclasts. After binding with RANK, its downstream signaling pathways regulate various functions [6]. During the process of osteoclastogenesis and activation, a minimum of five distinct signaling cascades mediated by protein kinases are initiated. These include the inhibitor of NF-κB kinase (IKK), c-Jun N-terminal kinase (JNK), p38, extracellular signal-regulated kinase (ERK), and Src pathways [7]. The combination of RANKL and RANK activates a unique signaling pathway that ultimately leads to the expression and nuclear translocation of NFATc1, a critical factor in regulating osteoclastogenesis [8].

Recent studies by Liu K and Zhang Y have indicated that natural compounds hold potential therapeutic effects on osteoclast-mediated osteolytic diseases [9,10]. Smilax china L., a member of the Liliaceae family commonly known as 'Baqia' in China, has been widely used by Zheng G, et al. in traditional Chinese medicine to treat various ailments such as rheumatic arthralgia and pelvic inflammation [11,12]. Modern pharmacological research revealed that Smilax china L. possesses various pharmacological activities, including anti-inflammatory [13], anticancer [14] and antioxidant properties, which protect the liver from damage [15]. Several bioactive molecules in Smilax china L. have been isolated and identified, with steroidal saponins and flavonoids being the main active ingredients [16,17]. Our previous work reported the isolation of several new structure steroidal saponins from Smilax china L., among which chongrenside D (CGD) showed significant anti-inflammatory activity by inhibiting LPS-induced TNF-α and IL-1β expression [18].

Wu D et al. indicated a very close correlations between chronic inflammation and bone diseases [19], the present work aimed to evaluate the pharmacological effects of CGD on RANKL-induced osteoclast differentiation and bone resorption function in vitro, as well as osteolysis induced by lipopolysaccharide (LPS) in an in vivo animal model.

2. Materials and methods

2.1. Media, reagents and antibodies

Chongrenside D was provided by Liwen Tian from the School of Pharmaceutical Sciences, Southern Medical University. Alpha Modification of Eagle's Medium (α-MEM), fetal bovine serum (FBS), penicillin and streptomycin for cell culture were obtained from Gibco (Rockville, MD, USA). Soluble recombinant mouse RANKL and M-CSF were purchased from Peprotech (Rocky Hill, NJ, USA). Hifair® 1st Strand cDNA Synthesis SuperMix and Hieff® qPCR SYBR Green MasterMix were sourced from TaKaRa (Dalian, China). Cell Counting Kit-8 (CCK-8) was acquired from Wuhan Yeasen Biotechnology Co., Ltd. (Wuhan, China). Hydroxyapatite-coated 96-well plates were bought from Corning Life Science (St. Lowell, MA, USA). Antibodies against Src, phospho-Src, MMP9, focal adhesion kinase (FAK), phospho-FAK, β3-Integrin, phospho-p38, p38, phospho-ERK1/2, ERK1/2, Akt phospho-JNK and JNK, NFATc1 (D15F1), GAPDH, and anti-NF-κB p65 (C22B4) rabbit mAb were all procured from Cell Signaling Technology (Danvers, MA, USA).

2.2. Primary cell culture

Eight-week-old male C57BL/6 mice (20–22g) were acquired from the Laboratory Animal Center of Southern Medical University. All experimental protocols were approved by the Institutional Animal Care and Use Committee of Southern Medical University.

Primary murine-derived bone marrow macrophages (BMMs) were harvested from the femur and tibia of the mice. Subsequently, these BMMs were cultured in complete α-MEM medium, containing 10 % FBS and a 1 % antibiotic mixture (penicillin and streptomycin), overnight.

2.3. Cytotoxicity assay

The CCK-8 assay was used to assess the cytotoxicity of CGD on BMMs. BMMs were adjusted to a cell density of $2x10^5$ cells/mL, re-suspended, and then incubated in a 96-well plate containing 25 ng/mL M-CSF and 10 % FBS (100 μL/well). After 2 days, non-adherent cells were discarded, fresh medium was added, and CGD was introduced at concentrations of 0, 0.5, 1, 2, and 3 μM. The cells were then cultured continuously for 72 h. Following this, the CCK-8 reagent was added and the cells were incubated for 3 h at 37 °C in a light-protected incubator. The absorbance was then measured at a wavelength of 450 nm using a microplate reader, and the cell viability of each group was standardized to the control.

2.4. Osteoclastogenesis and TRAP staining

BMMs were cultured in a 24-well plate at a density of 5×10^5 cells/mL using α-MEM medium supplemented with 25 ng/mL M-CSF and 10 % FBS for 2 days. Then the medium was replaced and 25 ng/mL M-CSF and 50 ng/ml RANKL were added to stimulate osteoclast differentiation for 6 days, and replaced the medium every 2 days [20].

After that, the culture medium was carefully discarded and the cells were washed three times with ddH_2O at 37 °C. The cells were then briefly immersed in TRAP fixative for 30 s, gently washed with ddH_2O at 37 °C, and incubated with staining buffer for 1 h at 37 °C in a light-protected incubator. Following a thorough wash with ddH_2O, hematoxylin was added for 2 min. The cells were then rinsed with tap water until the background was clear, and images were taken under a microscope for record-keeping. The number of cells with positive TRAP staining and $\geq$3 nuclei was determined. The sizes of the osteoclasts were measured using Image J software from ten arbitrarily chosen fields in each of the three independent experiments.

2.5. Bone resorption assay

BMM was cultured in Osteo Assay Strip well plate (St. Lowell, MA, USA) coated with apatite to mimic bone mineral fraction and cultured as described in our previous work [9]. After 6 days' stimulation, cells were then removed using a bleaching solution (10 %), and photographed using a microscope (Nikon, Tokyo, Japan). The resorption areas of each group were calculated using IPP software (Version 6.0, Media Cybernetics, USA).

2.6. Mouse model of LPS-induced bone loss

To assess the therapeutic efficacy of CGD, a mouse model of LPS-induced joint osteolysis was established following the National Institutes of Health Guide for Care and Use of Laboratory Animals (8th edition) and approved by the Southern Medical University Institutional Animal Care and Use Committee (SMUL2021080). Twenty-four 8-week-old male C57BL/6 mice were anesthetized with isoflurane, and LPS was dissolved in PBS to create a 100 μg/mL solution. A volume of 10 μL of LPS was then injected into the joint space of the knee or ankle. The contralateral (opposite) joint could be injected with an equal volume of sterile saline or PBS as a control [21].

The mice were randomly divided into four groups: sham (PBS), LPS (20 mg LPS/kg with PBS), low-dose (LPS with 5 mg CGD/kg), and high-dose (LPS with 10 mg CGD/kg). Preventive treatment was initiated one day before LPS administration, with PBS or CGD being injected every other day for 7 days. Finally, the mice were sacrificed humanely, and the joint tissues were collected and placed in 4 % PFA for further microcomputed tomography (micro-CT) and histological analysis.

2.7. Micro-CT

The high-resolution micro-CT was utilized for the analysis of the mouse paws under isometric resolution conditions of 18 μm and X-ray energy settings of 80 kV and 100 μA. Three-dimensional (3D) images were reconstructed using dedicated cone-beam software (SkyScan, Altestel, Belgium). The region of interest (ROI) encompassed a $3 \times 3 \times 1$ mm area centered on the midline suture, and was used to quantify osteolytic changes through measurements of bone volume to tissue volume ratio (BV/TV) and counting and measuring the area of holes.

2.8. Histological and immunohistochemical analysis

The bone tissues from each experimental group were carefully processed. Initially, they were fixed in 4 % PFA for two days, followed by a decalcification process using 10 % ethylenediaminetetraacetic acid for seven days. Subsequently, the samples were embedded in paraffin and sectioned for further morphometric examination. This involved staining procedures using hematoxylin and eosin (H&E), TRAP (procured from Sigma-Aldrich), and Safranine and Fast Green staining [11]. The prepared sections were then meticulously photographed under a microscope. Bone histomorphometric parameters such as Bone Volume/Total Volume (BV/TV), number of TRAP-positive osteoclasts (expressed as the number of osteoclasts on the bone surface, N.OC/B.S), osteoclast surface area per bone surface (OCs/BS), and Safranine-positive staining areas were measured using the Image-Pro Plus software (developed by

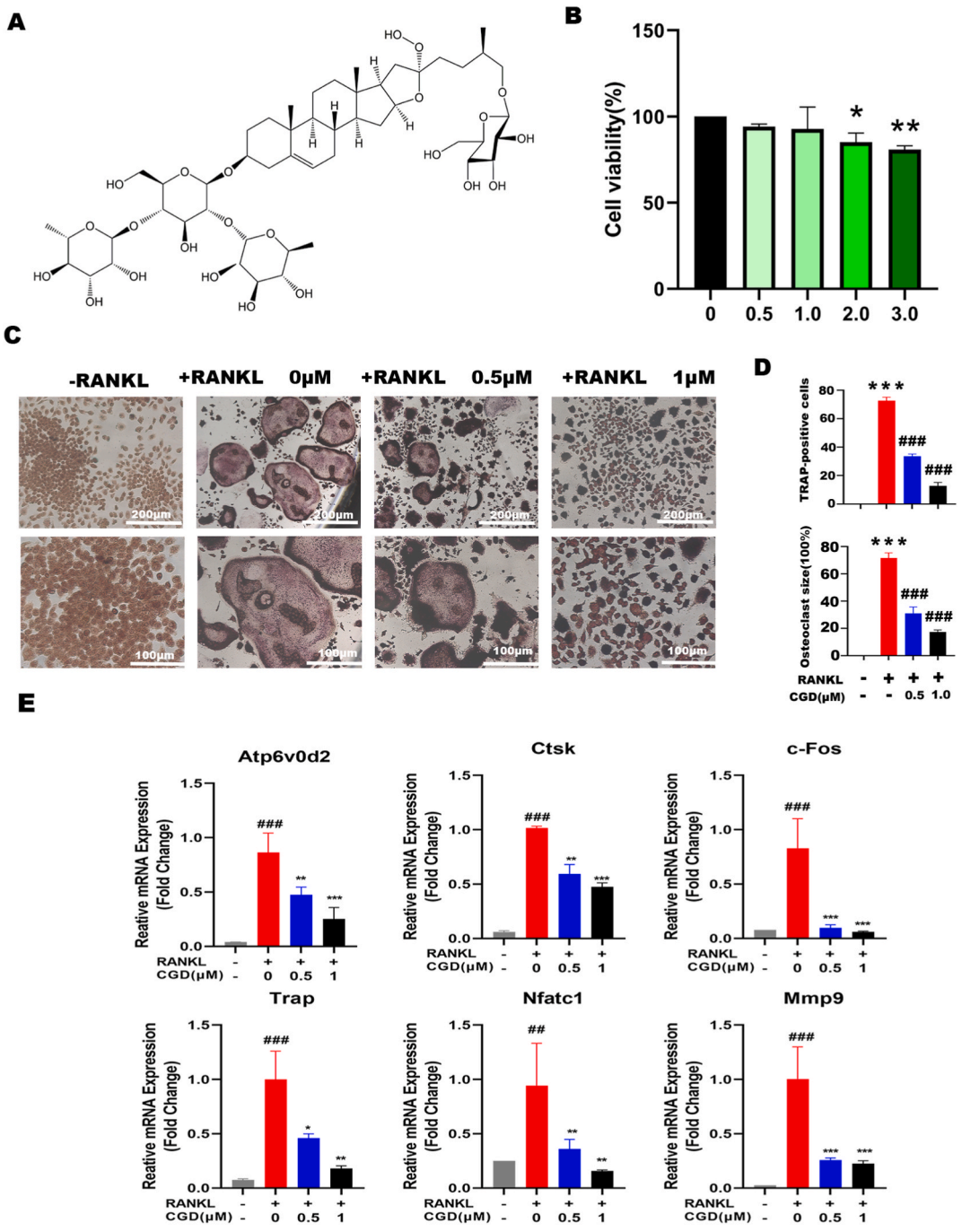

Fig. 1. CGD inhibits RANKL-induced osteoclast differentiation

(A) The Chemical structure of CGD, a furostanol saponin. Proceeded with treating Bone Marrow Macrophages (BMMs) with varying concentrations of CGD (0.5, 1.0, 2.0, and 3.0 μM) in a medium (α-MEM) enriched with 25 ng/ml M-CSF and 50 ng/ml RANKL. (B) CGD did not exhibit any cytotoxic effects on BMMs. (C) CGD demonstrates a dose-dependent inhibitory effect on the number and size of $TRAP^{+}$ giant multinucleated cells. (D) RANKL stimulation led the osteoclast-specific genes (TRAP, CtsK, MMP9, and β3-integrin) to a significant increase in mRNA levels while there were noticeably down-regulated by varying concentrations of CGD. (E) The expression of osteoclast biomarkers.

Media Cybernetics, Rockville, MD).

2.9. Real-time PCR

Bone marrow-derived mononuclear cells were plated in 6-well plates at a density of 10^6cells/well and stimulated with 50 ng/mL of RANKL for a period of five days. Total RNA was extracted using TRIeasy. A total of 1 μg of RNA was employed for the generation of cDNA. Following the reverse transcription stage, real-time PCR was conducted using SYBR qPCR Mix. All polymerase chain reaction (PCR) reactions were conducted using primers that were specific to the mouse sequence. Gene expression levels were calculated using the $2^{-\Delta\Delta CT}$ method.

2.10. Western blot analysis

After stimulation, total cell protein was harvested in RIPA buffer containing protease and phosphatase inhibitors, either with or without CGD. The protein concentration was determined using the BCA Protein Assay Kit. Each sample, with a total protein concentration of 20 μg/lane, was loaded and separated on a 10 % SDS-PAGE gel. Following this, the samples were transferred onto polyvinylidene difluoride membranes, which were then blocked with 5 % milk in TBST for 1 h. The blots were subsequently incubated with primary antibodies overnight at 4 °C, before being incubated with HRP-conjugated secondary antibodies for a further hour. Finally, the protein bands were analyzed using ImageJ software.

2.11. Gelatin zymography

The culture medium was harvested and the MMP9 activity was determined by a gelatinase zymography assay (Applygen, Beijing, China). An equal volume of supernatants (20 μL/lane) were separated by 8 % SDS-PAGE containing 10 mg gelatin. The sample was electrophoresed for 60 min at a constant current of 15 mA. Then the gels were washed twice with renaturing buffer for 30 min at RT and incubated with digestion buffer overnight at 37 °C. Following this, the gels were stained with Coomassie Brilliant Blue for 2 h, and were counter-stained with acetic acid and methanol. Images were captured using a gel documentation system.

2.12. Immunofluorescence staining

BMMs were cultured on 24-well coverslips at a density of 2×10^5 cells per well with M-CSF (25 ng/mL). Cells were initially treated with CGD (1 μM) for 2 h, followed by stimulation with RANKL (50 ng/mL) for 30 min. Afterward, the cells were fixed using 4 % (v/v) paraformaldehyde for 15 min at room temperature. A permeabilization process was then carried out using 0.5 % Triton X-100 for 5 min. Blocking was achieved using 10 % (v/v) normal goat serum (sourced from Invitrogen, Carlsbad, CA, USA) in PBS. Subsequently, the cells were subjected to rabbit primary antibodies against NF-κB p65 or NFATc1 for an hour at room temperature, followed by exposure to Alexa Fluor 594 goat anti-rabbit secondary antibody at a 1:2000 dilution in darkness for an hour. After thorough washing with PBS, the coverslips were mounted with DAPI in Prolong Gold anti-fade reagent and examined using a confocal microscope (manufactured by Nikon, Tokyo).

2.13. Statistical analysis

Results are expressed as mean ± standard deviation (SD). Statistical differences were determined by one-way ANOVA and Dunnett's post-test, and $p < 0.05$ was considered statistically significant.

3. Result

3.1. CGD inhibits RANKL-induced osteoclast differentiation

Our previous work demonstrated that CGD effectively inhibited the expression of inflammatory factors in Raw264.7 cells. As a result, we decided to delve deeper into its potential impact on osteoclast formation in vitro. We proceeded with treating Bone Marrow Macrophages (BMMs) with varying concentrations of CGD (0.5, 1.0, 2.0, and 3.0 μM) in a medium (α-MEM) enriched with 25 ng/ml M-CSF and 50 ng/ml RANKL (Chemical structure showed in Fig. 1A). As shown in Fig. 1B, CGD did not exhibit any cytotoxic effects on BMMs. However, it did demonstrate a dose-dependent inhibitory effect on the number and size of $TRAP^+$ giant multinucleated cells (Fig. 1C and D). The RANKL-induced upregulation of osteoclast-specific genes (TRAP, CtsK, MMP9, and β3-integrin) is a well-established contributor to osteoclast formation and bone resorption. Consequently, we aimed to determine whether CGD could suppress the expression of these key marker genes. As anticipated, RANKL stimulation led to a significant increase in mRNA levels, which were noticeably down-regulated by varying concentrations of CGD (Fig. 1E).

3.2. CGD inhibited actin ring formation and bone resorption

It is essential to understand the process of skeleton rearrangement, which occurs during the maturation of functional osteoclasts and results in bone resorption. This process is characterized by the formation of actin rings. As multinucleated osteoclasts adhere to the

bone surface, their membranes undergo polarization, leading to the secretion of hydrogen ions and lytic enzymes into the resorption pits to degrade the bone matrix. This specific region is encircled by a tight sealing band comprised of F-actin ring structures. As shown in Fig. 2A–B, the administration of CGD resulted in a notable reduction in the resorption pit area, which was attributed to a significant inhibition of mature osteoclast bone resorption activity. This was achieved by preventing the formation of F-actin rings (Fig. 2C).

3.3. CGD inhibited RANKL-stimulated protein expression

By attaching to the bone surface to form a resorption zone within a tight circumferential seal, osteoclasts fold into a pleated border. This attachment process is dependent on β3-integrin, Src and FAK molecules, thus to secrete acid hydrolases such as TRAP, CtsK, and MMP9. Consistent with gene expression data, RANKL stimulation significantly elevated protein levels of MMP-9 and the β3-integrin/Src/FAK axis, which were notably inhibited by CGD (Fig. 3A and B, Fig. 7A–B), as well as MMP9 activity (Fig. 3C and D). Similarly, the activation of the MAPK/AKT pathway, contributing to osteoclastogenesis and survival, was significantly reduced by CGD (Fig. 3E–F). CGD also inhibited MAPK/AKT pathway in the condition of short-time stimulation by RANKL (Fig. 3G and H).

3.4. CGD suppressed NFATc1/p65 nucleus translocation and MMP9 activity

Given the crucial role of NFATc1 and NF-κB signaling in osteoclast differentiation and bone resorption activity, we investigated if CGD could also impair osteoclastogenesis by inhibiting NFATc1 and p65 nuclear translocation. As depicted in Fig. 4A–D, CGD notably decreased the nuclear fluorescence of NFATc1 and p65 compared to RANKL-stimulated cultures, demonstrating CGD's ability to inhibit RANKL-induced osteoclastogenesis by impairing the activation of the associated transcription factors NFATc1 and NF-κB.

3.5. CGD protected joint from erosion and inflammation in LPS-induced bone loss mice model

The potential protective effect of CGD on pathological osteolysis was further explored in vivo, using a mouse model of LPS-induced

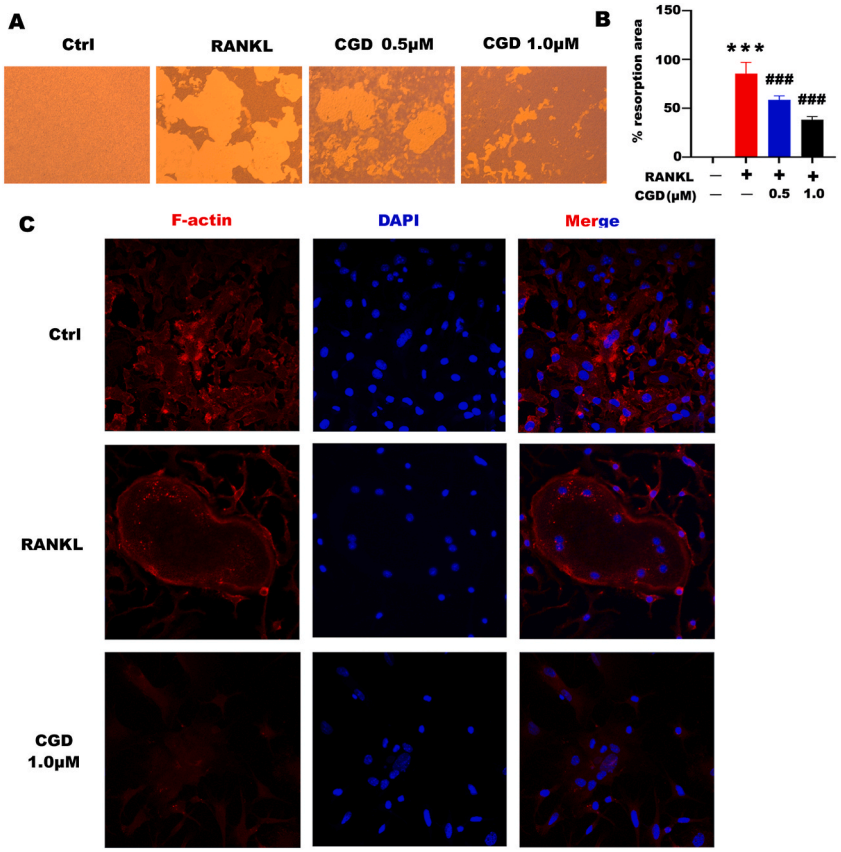

Fig. 2. Effect of CGD on actin ring formation and bone resorption
(A-B) Topography of resorbed area was reconstructed and the ratio of the resorption area to the total area of hydroxyapatite-coated surface was analyzed by Image J. Data are means ± SD, from ten independent views. (C) Immunofluorescence staining of F-acting in mature osteoclasts. ***P < 0.001 vs Control group, ###p < 0.001 vs RANKL group.

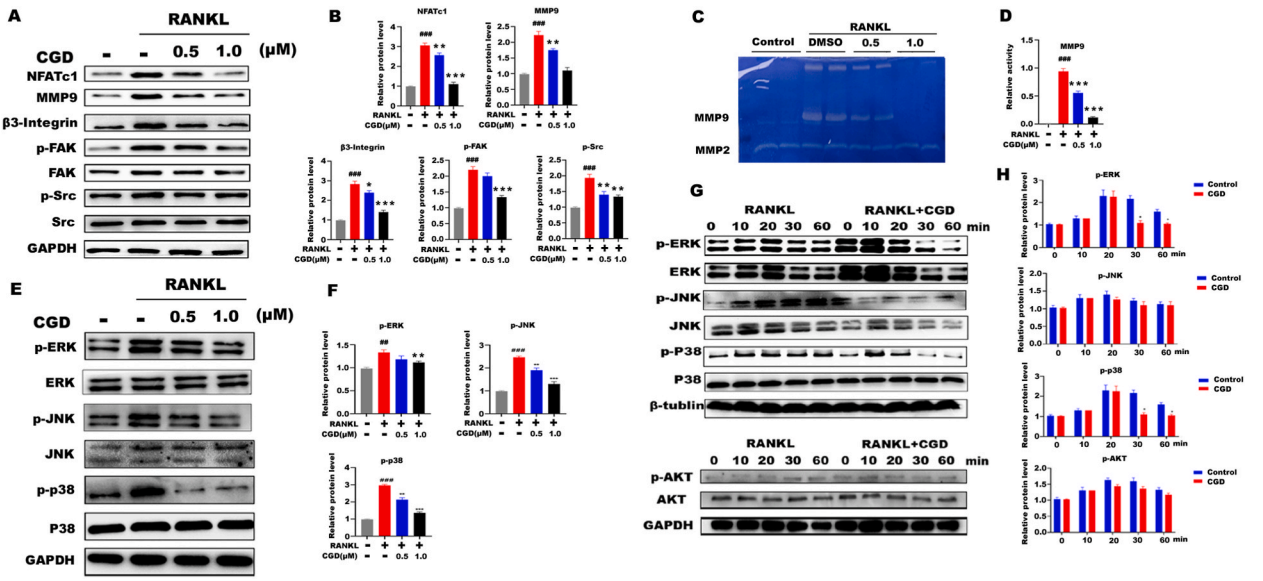

Fig. 3. CGD inhibited RANKL-stimulated protein expression

(A-B) Western blot analysis of osteoclasts with CGD or not to evaluate the protein levels of MMP-9 and the β3-integrin/Src/FAK axis. (C, D) MMP9 activity assay of culture medium from osteoclasts treated with or without CGD by gelatin zymography. (E, F) Western blot analysis of osteoclasts with CGD or not to evaluate the protein level of p-JNK, JNK, p-ERK, ERK, p-p38, p38, GAPDH, n = 3. (G, H) Western blot analysis of BMM stimulated with 50 ng/mL RANKL in the condition of CGD or not for indicated time to evaluate the protein expression of MAPK and AKT pathway. Data are presented as means ± SD, ##p < 0.01, ###P < 0.001 vs Control group, *p < 0.05, **p < 0.01, ***p < 0.001 vs RANKL group.

bone loss. CT images revealed significant bone loss induced by LPS, which was notably mitigated by CGD treatment, particularly in the 20 mg/kg CGD group (Fig. 5A). Compared to the sham group, the LPS-treated group displayed significant reductions in Tb.Th, Tb.N, BV/TV values, and BMD, with a marked increase in Tb.Sp. However, CGD treatment significantly and dose-dependently counteracted these decreases (Fig. 5B). Elisa and PCR data highlighted CGD's ability to inhibit the release of inflammatory factors such as TNF-α, IL-4, IL-6, and IL-10 (Fig. 5D). Additional data demonstrated that CGD dose-dependently increased BV/TV (Fig. 5B) and decreased the number of TRAP-positive cells (Fig. 5C).

The histological and histomorphometric analysis further supported CGD's protective role against LPS-induced osteolysis (Fig. 6A and B). Safranine and Fast Green staining images showed a significant improvement in the structure of articular cartilage, subchondral bone, and bone tissue after CGD treatment (Fig. 6C). TRAP staining of the joints also indicated that the CGD groups had significantly reduced TRAP-positive areas (Fig. 6D–E). Data from mRNA analysis showed consistent results, CGD inhibited the marker genes level of osteoclasts, such as NFATc1, CtsK, c-Fos and Atp6v0d2. Meanwhile, CGD downregulated the expression of the pro-inflammatory factors TNF and IL-6, but upregulated the level of the anti-inflammatory factors IL-4 and IL-10 (Fig. 7C).

4. Discussion

Bone-destructive diseases pose a significant challenge to the maintenance of bone homeostasis and usually enhance bone resorption and increase the number of osteoclasts, leading to bone-destructive conditions like osteoporosis and rheumatoid arthritis [22]. The current therapeutic options mainly target vesicle trafficking by inhibiting the release of specific enzymes into the sealing zone, thus suppressing its bone-resorption function [23]. Nonsteroidal anti-inflammatory drugs (NSAIDs) or glucocorticoids are usually used to decrease inflammatory cytokines but cannot stop the progression of the disease, especially bone erosion [24]. A promising candidate is Denosumab, a specific antibody to RANK, which holds potential for treating osteonecrosis of the jaw and atypical fractures, but still shows serious side effects and cannot reduce inflammation [25]. Given the dearth of efficacious and tolerable therapeutic options for bone-destructive diseases, Liang B presented that it is imperative to investigate novel treatment modalities [26]. In this work, we found that CGD significantly inhibited RANKL-induced osteoclast formation, bone resorption activity. These findings suggest that CGD plays a crucial role in preventing or mitigating RANKL-mediated osteolytic bone disease, offering a promising therapeutic avenue for these conditions.

Cytokines and/or chemokines, IL-1β, IL-6 and TNF-α are thought to be important factors associated with joint destruction in osteoarthritis by Martel-Pelletier J [27]. In our previous work, we reported that CGD significantly inhibited the expression of LPS-induced TNF-α and IL-1β, thus demonstrating substantial anti-inflammatory activity [18]. In this context, we expanded our investigation to consider the role of CGD in the disruption of bone homeostasis in rheumatoid arthritis, beyond its inflammatory aspects. Our findings revealed that CGD presented remarkable effects both in anti-inflammatory and anti-osteolysis. The anti-inflammatory effects of CGD were demonstrated by ELISA and PCR assay, which indicated the reduced secretion of

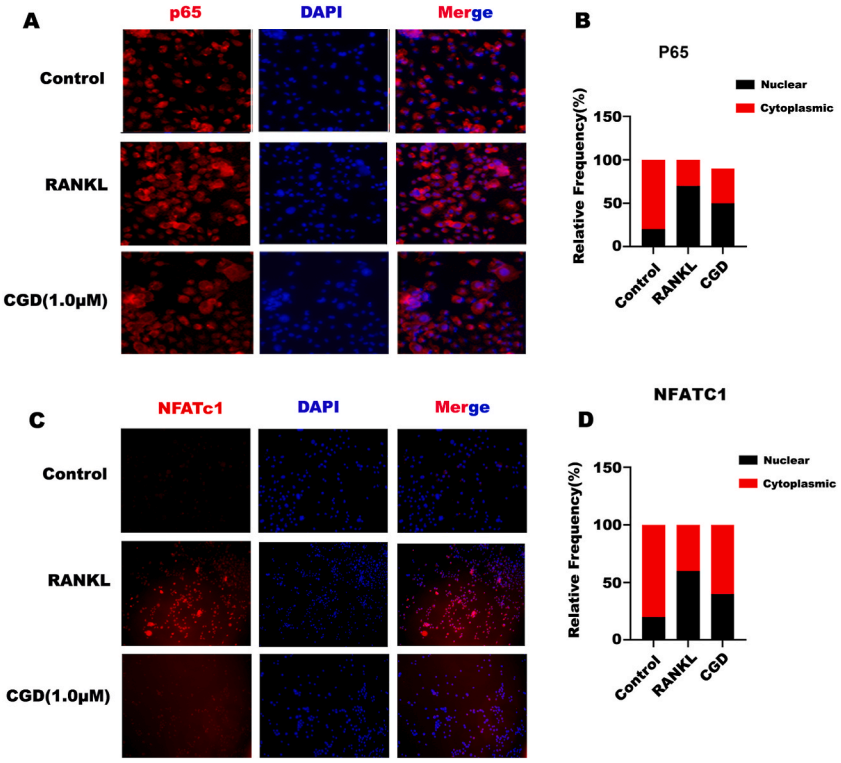

Fig. 4. CGD suppressed NFATc1/p65 nucleus translocation and MMP9 activity.
(A, B) Immunofluorescence of BMM treated with CGD or not for p65 and nucleus with p65 antibody and DAPI respectively. BMM were cultured in 24-well plates with glass coverslips stimulated with 50 ng/ml RANKL for 12h. (C, D) Immunofluorescence of BMM treated with CGD or not for NFATc1 and nucleus with NFATc1 antibody and DAPI respectively. BMM were cultured in 24-well plates with glass coverslips stimulated with 50 ng/ml RANKL for 12h, n = 6.

pro-inflammatory cytokines such as TNF-α, IL-4, and IL-6 and restored levels of the anti-inflammatory cytokine IL-10. Supporting this, histomorphological analyses and other data also verified the protective function of CGD on LPS-induced bone loss in vivo, thereby highlighting its therapeutic potential in the context of osteolytic diseases.

The formation and function of osteoclasts are determined by the expression levels of related target genes, including TRAP, CTSK, and MMP-9. These influence osteoclast secretion and bone resorption activities, while β3-integrin influences osteoclast migration and adhesion [28]. The results of our experiment demonstrated that CGD exerts an inhibitory effect on RANKL-induced osteoclast differentiation. This finding was further corroborated by the observation that CGD inhibited the expression of RANKL-stimulated proteins. Conversely, CGD treatment also significantly reduced the level of inflammation in the body, exhibiting a similar effect to that of NSAIDs.

Lorenzo J used to report the importance of NFATc1 and NF-κB signaling in osteoclast differentiation and bone resorption activity [29]. Our study also revealed that CGD inhibited NFATc1/p65 nuclear translocation and the activity of MMP9. Fang Q also mentioned that the activation of MAPKs and Akt pathways also plays a crucial role in cell proliferation and osteoblastogenesis [30]. CGD exhibited a significant reduction in RANKL-induced phosphorylation levels of Akt, JNK, and p38, but not ERK. This observation suggests that the inhibitory effect of CGD on the phosphorylation of Akt, p38, and JNK may contribute to the regulation of MAPK activation within osteoclasts. The exclusion of ERK might be the reason why CGD didn't show cytotoxicity in BMMs within 3 μM.

5. Conclusion

Coupling with our current results that CGD effectively impedes RANKL-induced osteoclast differentiation and function, thus exerting its anti-osteoclast activity both in vitro and in vivo, it is suggested that CGD holds immense potential for the prevention and treatment of RANKL-mediated osteolytic bone diseases. Although our study presents valuable findings, it is not without limitations. The models commonly utilized for examining bone destruction are the collagen-induced arthritis model and the osteoporosis model. This was because intense inflammation is a significant contributing factor to bone destruction. Furthermore, our results demonstrated that CGD has a strong inhibitory effect on osteoclast differentiation in vitro. However, its in vivo effects are primarily reflected in its anti-inflammatory properties. This discrepancy could be associated with our use of an acute inflammatory model. In future research, it might be beneficial to examine the effects of CGD on bone destruction using other models, such as the collagen-induced arthritis model or the osteoporosis model, as well as verifying the direct biological target.

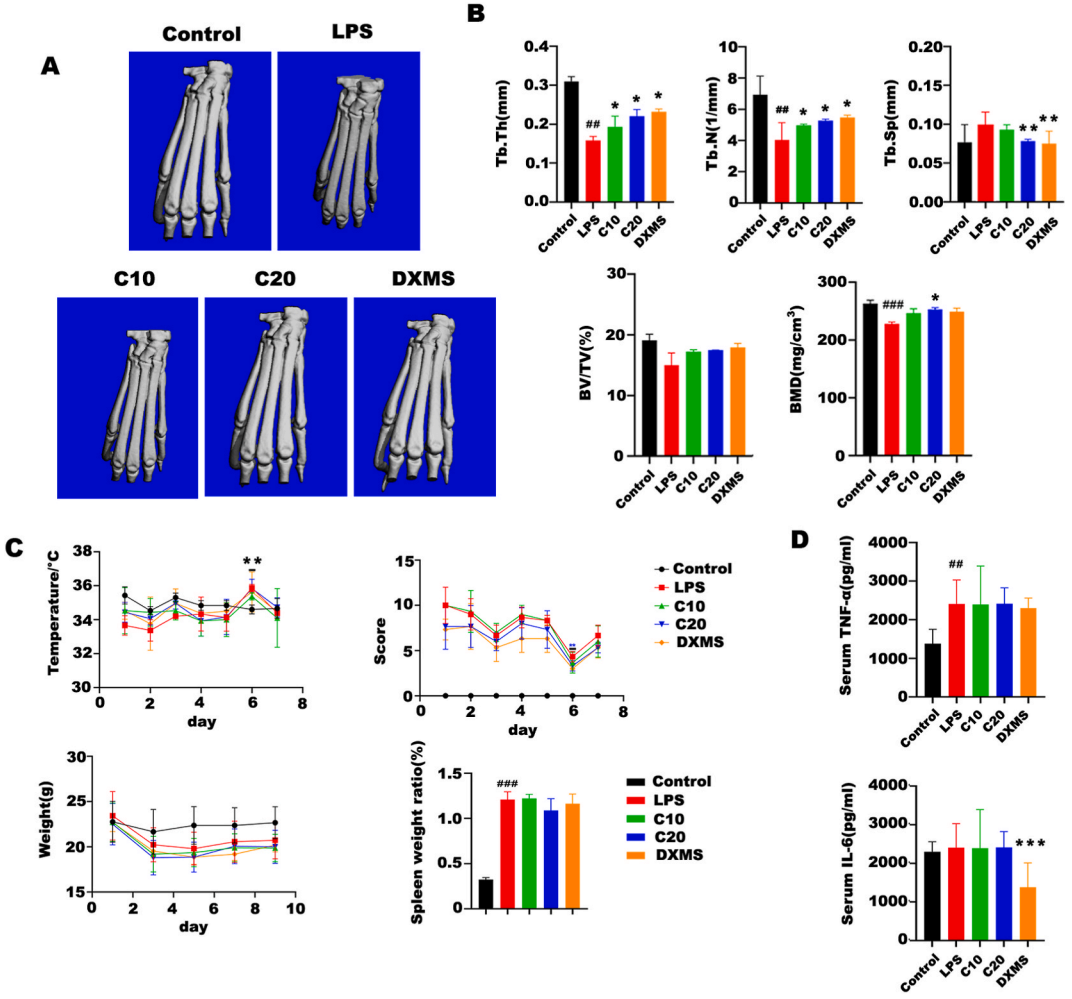

Fig. 5. CGD protected joint from erosion and inflammation in LPS-induced bone loss mice model
(A) CT images revealed significant bone loss induced by LPS, which was notably mitigated by CGD treatment, particularly in the 20 mg/kg CGD group. (B) Compared to the sham group, the LPS-treated group displayed significant reductions in Tb.Th, Tb.N, BV/TV values, and BMD, with a marked increase in Tb.Sp. These decreases were significantly and dose-dependently inhibited by CGD treatment. (C) Records of individual indicators used to assess disease such as Temperature, Weight, etc. (D) Elisa and PCR data highlighted CGD's ability to inhibit the release of inflammatory factors such as TNF-α, IL-4, IL-6, and IL-10. Data are presented as means ± SD, ##p < 0.01, ###P < 0.001 vs Control group, *p < 0.05, vs LPS group.

Ethics approval and consent to participate

The animal study was reviewed and approved by the Ethics Committee of Southern Medical University (SMUL2021080).

Consent for publication

Not applicable.

Funding

This study was supported by Sanming Project of Medicine in Shenzhen (No. SZZYSM202206005), Shenzhen Bao'an Traditional Chinese Medicine Hospital Research Program (No. BAZYY20200603), Guangdong Basic and Applied Basic Research Foundation (No.2019A1515111192, 2022A1515012297), Science and Technology Program of Guangzhou, China (No.2024A03J0857), Research project of Guangdong Provincial Bureau of Traditional Chinese Medicine (20211161), Project of Traditional Chinese Medicine Bureau of Guangdong province (No. 20221016) and Guangdong Hospital Pharmacy Research Foundation (No. 2023A01).

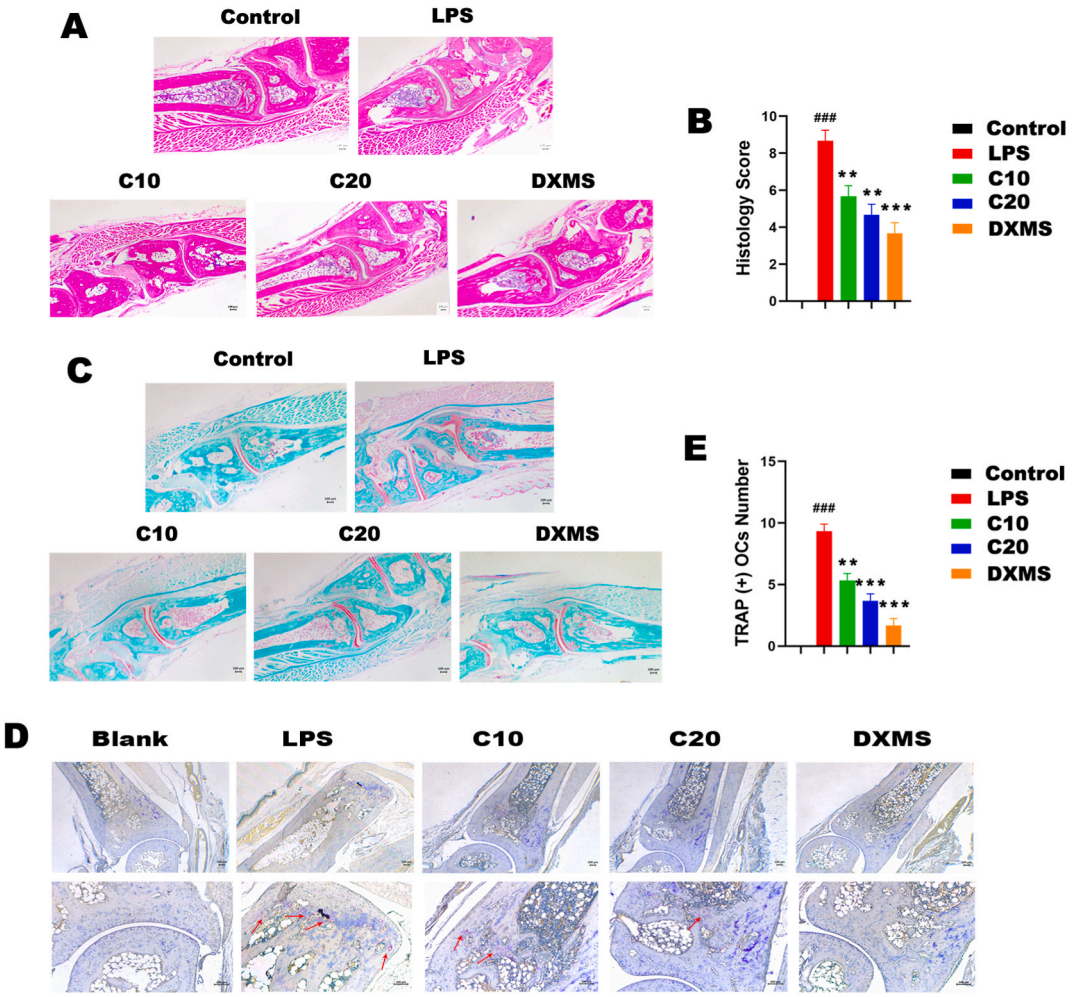

Fig. 6. CGD protected against joint damage and inhibited osteoclast formation in mice
(A, B) Hematoxylin and eosin (H&E) staining of joint bone tissues and the histology score. (C) Safranine and Fast Green staining of bone tissues. (D, E) TRAP staining and $TRAP^{+}$ OCs number for each group.

Data availability statement

The data that support the findings of this study are available from the corresponding author, upon reasonable request.

CRediT authorship contribution statement

Yanxiang Liang: Writing – original draft, Methodology, Data curation, Conceptualization. **Tian Qin:** Writing – original draft, Investigation, Formal analysis, Conceptualization. **Caixia Pang:** Project administration, Methodology, Formal analysis. **Xinru Yang:** Validation, Software, Investigation. **Zongbin Wu:** Supervision, Resources. **Xiaolian Liao:** Validation, Methodology. **Jie Zhang:** Validation, Software, Funding acquisition. **Siyu Zeng:** Resources, Project administration, Funding acquisition. **Chun Zhou:** Writing – review & editing, Supervision, Project administration. **Cuiling Liu:** Writing – review & editing, Supervision, Methodology, Funding acquisition.

Declaration of competing interest

The authors declare the following financial interests/personal relationships which may be considered as potential competing interests:

Cuiling Liu reports financial support was provided by Sanming Project of Medicine in Shenzhen. Cuiling Liu reports financial support was provided by Shenzhen Bao'an Traditional Chinese Medicine Hospital Research Program. Cuiling Liu, Chun Zhou reports financial support was provided by Guangdong Basic and Applied Basic Research Foundation. Siyu Zeng reports financial support was

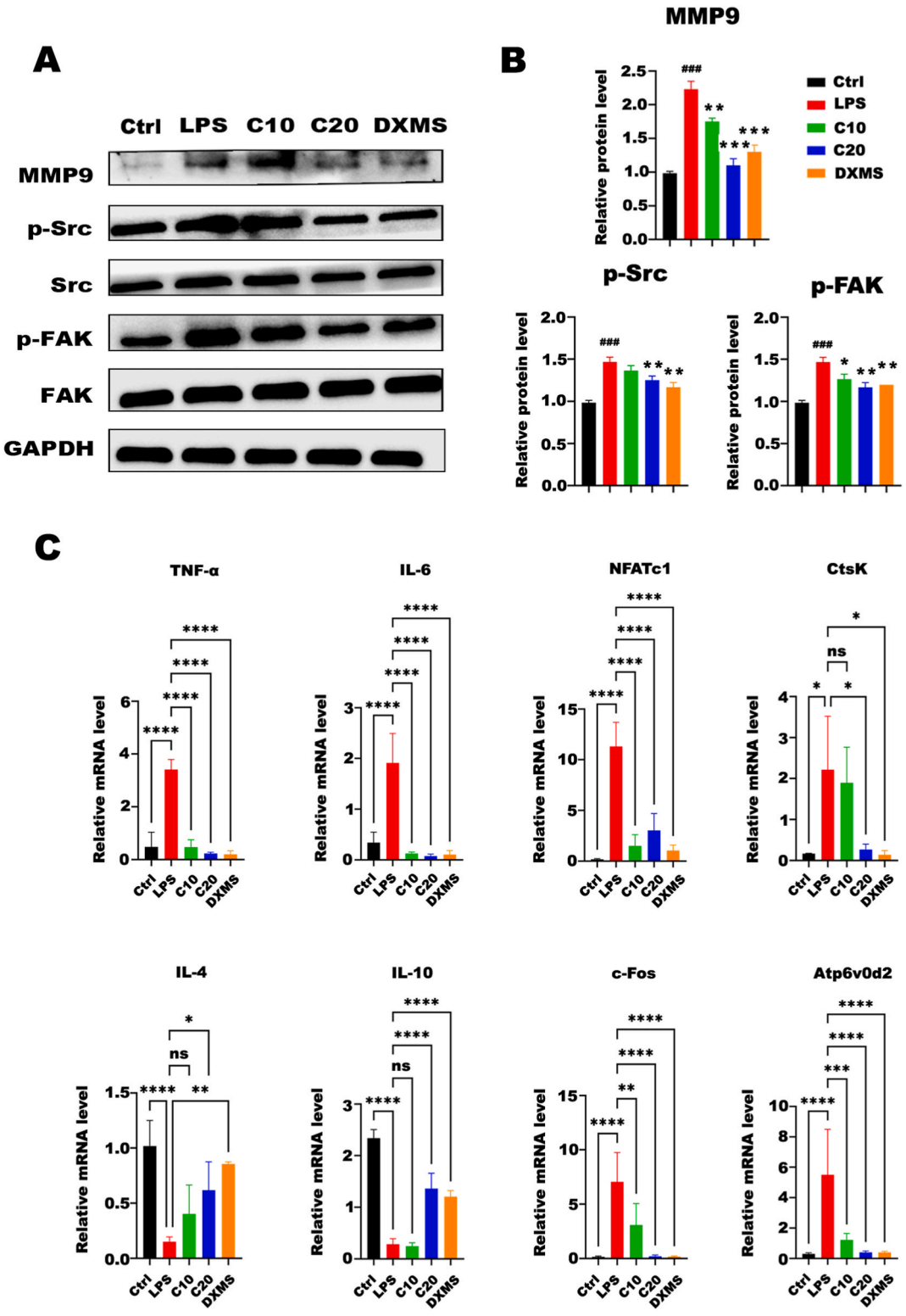

Fig. 7. CGD significantly inhibited the inflammatory response induced by LPS.
(A–B) Western Blot analysis of MMP-9, p-Src, Src, p-FAK, FAK levels in the bone tissues. (C) The mRNA expression of TNF-α, IL-4, IL-6, IL-10, Nfatc1, Ctsk, c-Fos, Atp6v0d2 signaling pathways was analyzed by q-PCR. Data are presented as means ± SD, ###P < 0.001 vs Control group, *p < 0.05, **p < 0.01, ***p < 0.001 vs LPS group.

provided by Science and Technology Program of Guangzhou. Jie Zhang, Siyu Zeng reports financial support was provided by Research project of Guangdong Provincial Bureau of Traditional Chinese Medicine. Siyu Zeng reports financial support was provided by Guangdong Hospital Pharmacy Research Foundation. If there are other authors, they declare that they have no known competing financial interests or personal relationships that could have appeared to influence the work reported in this paper.

Acknowledgment

We thank Prof. Liwen Tian from School of Pharmaceutical Sciences, Southern Medical University for providing CGD used in this article.

Appendix A. Supplementary data

Supplementary data to this article can be found online at https://doi.org/10.1016/j.heliyon.2024.e38818.

References

[1] J. Tuckermann, R.H. Adams, The endothelium-bone axis in development, homeostasis and bone and joint disease, Nat. Rev. Rheumatol. 17 (10) (2021) 608–620.
[2] B.L. Langdahl, Overview of treatment approaches to osteoporosis, Brit J Pharmacol 178 (9) (2021) 1891–1906.
[3] C. Zhou, Y. You, W. Shen, Y.Z. Zhu, J. Peng, H.T. Feng, et al., Deficiency of sorting nexin 10 prevents bone erosion in collagen-induced mouse arthritis through promoting NFATc1 degradation, Ann. Rheum. Dis. 75 (6) (2016) 1211–1218.
[4] Y. Xu, H. Tan, K. Liu, C. Wen, C. Pang, H. Liu, et al., Targeted inhibition of ATP5B gene prevents bone erosion in collagen-induced arthritis by inhibiting osteoclastogenesis, Pharmacol. Res. 165 (2021).
[5] W.J. Boyle, W.S. Simonet, D.L. Lacey, Osteoclast differentiation and activation, Nature 423 (6937) (2003) 337–342.
[6] D.J. Veis, C.A. O'Brien, Osteoclasts, master sculptors of bone, Annu. Rev. Pathol. 18 (2023) 257–281.
[7] J.H. Park, E. Jeong, J. Lin, R. Ko, J.H. Kim, S. Yi, et al., RACK1 interaction with c-Src is essential for osteoclast function, Exp. Mol. Med. 51 (7) (2019) 1–9.
[8] C. Zhou, Y. You, W.X. Shen, Y.Z. Zhu, J. Peng, H.T. Feng, et al., Deficiency of sorting nexin 10 prevents bone erosion in collagen-induced mouse arthritis through promoting NFATc1 degradation, Ann. Rheum. Dis. 75 (6) (2016) 1211–1218.
[9] J. Peng, K. Zhao, J. Zhu, Y. Wang, P. Sun, Q. Yang, et al., Sarsasapogenin suppresses RANKL-induced osteoclastogenesis in vitro and prevents lipopolysaccharide-induced bone loss in vivo, Drug Des. Dev. Ther. 14 (2020) 3435–3447.
[10] K. Liu, Y. Liu, Y. Xu, K.S. Nandakumar, H. Tan, C. He, et al., Asperosaponin VI protects against bone destructions in collagen induced arthritis by inhibiting osteoclastogenesis, Phytomedicine 63 (2019).
[11] Y. Zhang, X. Pan, S. Ran, K. Wang, Purification, structural elucidation and anti-inflammatory activity *in vitro* of polysaccharides from *Smilax china* L, Int. J. Biol. Macromol. 139 (2019) 233–243.
[12] H. Feng, Y. He, L. La, C. Hou, L. Song, Q. Yang, et al., The flavonoid-enriched extract from the root of *Smilax china* L. inhibits inflammatory responses via the TLR-4-mediated signaling pathway, J. Ethnopharmacol. 256 (2020).
[13] X. Li, L. Chu, S. Liu, W. Zhang, L. Lin, G. Zheng, *Smilax china* L. flavonoid alleviates HFHS-induced inflammation by regulating the gut-liver axis in mice, Phytomedicine 95 (2022).
[14] C. Wang, Q. Zhou, S.T. Wu, Scopolin obtained from Smilax China L. against hepatocellular carcinoma by inhibiting glycolysis: a network pharmacology and experimental study, J. Ethnopharmacol. 296 (2022) 115469.
[15] K. Wang, L. Yang, J. Zhou, X. Pan, Z. He, J. Liu, et al., *Smilax china* L. Polysaccharide alleviates oxidative stress and protects from acetaminophen-induced hepatotoxicity *via* activating the Nrf2-ARE pathway, Front. Pharmacol. 13 (2022).
[16] Y.-L. Li, G.-P. Gan, H.-Z. Zhang, H.-Z. Wu, C.-L. Li, Y.-P. Huang, et al., A flavonoid glycoside isolated from *Smilax china* L. rhizome *in vitro* anticancer effects on human cancer cell lines, J. Ethnopharmacol. 113 (1) (2007) 115–124.
[17] C. Zhang, S. Feng, L. Zhang, Z. Ren, A new cytotoxic steroidal saponin from the rhizomes and roots of Smilax scobinicaulis, Nat. Prod. Res. 27 (14) (2013) 1255–1260.
[18] Y. Xie, D. Hu, C. Zhong, K.-F. Liu, E. Fang, Y.-J. Zhang, et al., Anti-inflammatory furostanol saponins from the rhizomes of *Smilax china* L, Steroids 140 (2018) 70–76.
[19] D. Wu, A. Cline-Smith, E. Shashkova, A. Perla, A. Katyal, R. Aurora, T-cell mediated inflammation in postmenopausal osteoporosis, Front. Immunol. 12 (2021).
[20] H. Tan, L. Ma, T. Qin, K. Liu, Y. Liu, C. Wen, et al., Myo6 mediates osteoclast function and is essential for joint damage in collagen-induced arthritis, Biochim. Biophys. Acta, Mol. Basis Dis. 1870 (1) (2024) 166902.
[21] X. Zhu, J. Gao, P.Y. Ng, A. Qin, J.H. Steer, N.J. Pavlos, et al., Alexidine dihydrochloride attenuates osteoclast formation and bone resorption and protects against LPS-induced osteolysis, J. Bone Miner. Res. : the official journal of the American Society for Bone and Mineral Research 31 (3) (2016) 560–572.
[22] Á. Szentpétery, Á. Horváth, K. Gulyás, Z. Pethö, H.P. Bhattoa, S. Szántó, et al., Effects of targeted therapies on the bone in arthritides, Autoimmun. Rev. 16 (3) (2017) 313–320.
[23] M.R. Allen, Recent advances in understanding bisphosphonate effects on bone mechanical properties, Curr. Osteoporos. Rep. 16 (2) (2018) 198–204.
[24] J.N. Katz, K.R. Arant, R.F. Loeser, Diagnosis and treatment of hip and knee osteoarthritis: a review, JAMA 325 (6) (2021) 568–578.
[25] I.R. Reid, E.O. Billington, Drug therapy for osteoporosis in older adults, Lancet (London, England) 399 (10329) (2022) 1080–1092.
[26] B. Liang, G. Burley, S. Lin, Y.C. Shi, Osteoporosis pathogenesis and treatment: existing and emerging avenues, Cell. Mol. Biol. Lett. 27 (1) (2022) 72.
[27] J. Martel-Pelletier, A.J. Barr, F.M. Cicuttini, P.G. Conaghan, C. Cooper, M.B. Goldring, et al., Osteoarthritis, Nat. Rev. Dis. Prim. 2 (2016) 16072.
[28] D. Zhao, B. Shu, C. Wang, Y. Zhao, W. Cheng, N. Sha, et al., Oleanolic acid exerts inhibitory effects on the late stage of osteoclastogenesis and prevents bone loss in osteoprotegerin knockout mice, J. Cell. Biochem. 121 (1) (2020) 152–164.
[29] J. Lorenzo, The many ways of osteoclast activation, J. Clin. Invest. 127 (7) (2017) 2530–2532.
[30] Q. Fang, C. Zhou, K.S. Nandakumar, Molecular and cellular pathways contributing to joint damage in rheumatoid arthritis, Mediat. Inflamm. 2020 (2020) 3830212.